$L > 2D$. (3) A filopodium that is a long filamentous protrusion with no distinguishable head. L is much longer than the neck diameter (d). (4) A stubby spine that does not have a distinguishable head, and has an L-value similar to d. The significance of the drug effect was examined using the Tukey–Kramer posthoc multiple comparisons test when one way ANOVA tests yielded $p < 0.05$.

RC-19 antibody preparation and purification

MC-20 is a widely used antiserum against the C-terminal of ERα, but it has serious problems in non-specific staining of ERα in the hippocampus of ERalphaKO mice. Therefore, purification of ERα-specific antibody fractions from antiserum was necessary. As purification of ERα-specific antibody fractions requires a large amount of antiserum, we prepared home-made purified antibody RC-19. The most C-terminal 19 amino acids (C-HSLQTYYIP-PEAEGFPNTI) of rat ERα conjugated with bovine serum albumin (BSA) via *m*-maleimidobenzoyl-*N*-hydroxysuccinimide ester (Sigma) were used as an antigen. Antibody was elicited in male white rabbits. A 40 ml aliquot of the collected sera from the rabbits was passed through a BSA immobilized Sepharose 4B column (1 × 5.5 cm) containing 5 mg BSA to remove the antibody against BSA. Subsequently, the specific antibody against the peptide was adsorbed on the peptide-BSA immobilized Sepharose 4B column (1 × 2 cm). The column was washed with 30 mL of 50 mM potassium phosphate buffer (pH 7.2) containing 1% (w/v) sodium cholate and 500 mM NaCl. RC-19 antibody was eluted with 100 mM glycine (pH 4.0) containing 0.15 M NaCl. The pH of the eluted antibody was adjusted to pH 7.4 by immediate mixing with 1 M Tris-HCl (pH 8.0) to prevent denaturation of antibody. The elution was performed within 30 min. Purified RC-19 was stored at − 80°C, with 0.5% BSA, in many separate tubes with a small volume. Once a tube of fresh antibody had been used after thawing we never re-froze it for further use, but discarded it. Repetitive thawing and freezing of antibody should be avoided, otherwise the good immunoreactivity of RC-19 in hippocampal tissues is lost.

Preparation of synaptic, cytoplasmic and nuclear fractions

The same hippocampal slices were used in order to compare the results obtained with electrophysiology and spine morphology investigations. For western blot of hypothalamus, cerebral cortex and cerebellum, whole tissues of these brain regions (instead of slices) were used. Fractionation was performed by a combination of centrifugations at 4°C for the hippocampus, hypothalamus, cerebral cortex and cerebellum (Cohen *et al.* 1977). Detailed descriptions of centrifugation procedures to obtain the nuclear fraction, the PSD fraction, the presynaptic membrane-enriched fraction and the cytoplasmic fraction are described in *Supplementary Material*.

Western immunoblot analysis

Purified fractions prepared by centrifugation were suspended in 125 mM Tris-HCl buffer (pH 6.8) containing 5 mM 2-mercaptoethanol, 10% sucrose, 6% sodium dodecylsulfate (SDS) and 0.002% bromophenol blue. The fractions were subjected to electrophoresis using a 10% polyacrylamide gel. After transfer to polyvinylidene fluoride membranes (Immobilon-P; Millipore Co., Bedford, MA, USA), the blots were probed with purified antibody RC-19 (diluted to 1/2000), MC-20 antiserum (1/3000) or AS409 antiserum (1/2000, a gift from Prof. Shinji Hayashi) for 12–18 h at 4°C, and incubated with horseradish peroxidase (HRP)-conjugated goat anti-rabbit IgG (Cell Signaling). The protein bands were detected with enhanced chemiluminescence (ECL) plus western blotting detection reagents (Amersham, Piscataway, NJ, USA). To obtain high quality images of chemiluminescence from protein bands using ECL plus, we used LAS3000 Image Analyzer (Fuji Film) with a 16-bit wide dynamic range.

Immunohistochemical staining of hippocampal slices

Immunohistochemical staining was performed essentially as described elsewhere (Kimoto *et al.* 2001; Kawato *et al.* 2002). Briefly, hippocampal slices were prepared from a rat or mouse deeply anesthetized with pentobarbital and perfused transcardially with PBS (0.1 M phosphate buffer and 0.14 M NaCl, pH 7.3), followed by fixative solution of 4% paraformaldehyde. The hippocampi were post-fixed, cryoprotected and frozen-sliced coronally at 20 μm thickness with a cryostat (Leica CM1510, Germany). Brains from several animals were used and from each brain, a single representative coronal section including the dorsal hippocampus was selected.

Staining for ERα was performed using the avidin-biotin peroxidase complex (ABC) technique. RC-19 was pre-treated with 5% BSA for 5 h to pre-absorb non-specific contaminated IgGs against BSA. After application of RC-19 IgG (1/1000) or MC-20 antiserum (1/500), the slices were incubated for 24 h at 4°C, in the presence of 0.5% Triton X-100 and 3% skim milk, with gentle shaking. Triton X-100 treatment was necessary to facilitate penetration of IgGs into cells in slices. Biotinylated anti-rabbit IgG (1/1000) in PBS was then applied, followed by a 30 min incubation with streptavidin-horseradish peroxidase complex (Vector Laboratories, Burlingame, CA, USA). Immunoreactive products were detected by immersing the slices in a detection solution (0.1 M Tris-HCl, pH 7.2, containing 0.05% diaminobenzidine, 0.1% H_2O_2 and 0.3% ammonium nickel sulfate). After dehydration and embedding in Entellan Neu (Merck), the immunoreactive cells in the slices were examined under a microscope, and digital images with a 2272 × 1704 pixel resolution were taken by a digital camera (COOLPIX4500, Nikon). For pre-absorption of RC-19 with antigen, excess amount of antigen was pre-incubated with RC-19 for 15 h at 4°C.

Post-embedding immunogold method for electron microscopy

Rat hippocampal slices were prepared in essentially the same manner as that used for the immunohistochemical staining, except that slicing was performed at 4°C using a vibratome instead of frozen slicing. Brains from five animals were used and from each brain, a single representative coronal section including the dorsal hippocampus was processed for ultrathin sectioning. Freeze substitution and low-temperature embedding of the specimens was performed as described previously (Adams *et al.* 2002). Briefly, slices were plunged into liquid propane. The samples were immersed in uranyl acetate in anhydrous methanol (− 90°C), then infiltrated with Lowicryl HM20 resin (Electron Microscopy Sciences, USA); polymerization was performed with ultraviolet light. Ultrathin sections were cut using a Reichert-Jung ultramicrotome. For immunolabeling, sections were incubated with primary antibody for RC-19 (1/1000) or MC-20 (1/2000) in the above diluent overnight, then incubated with secondary gold-tagged (10 nm) Fab

fragment in Tris-buffered saline (TBS). Sections were counter-stained with 1% uranyl acetate, and viewed on a JEOL 1200EX electron microscope (Japan). Images were captured using the CCD camera (Advanced Microscopy Techniques, USA). Controls omitting the primary antibody were performed and no immunogold labeling was observed.

Mass spectrometric analysis of RC-19 reacted ERα

To perform immunoprecipitation with RC-19, a hippocampal cytoplasmic fraction (1 mg/mL) was suspended 5 mM HEPES buffer. A 20 μL volume of protein-G-Sepharose beads (Sigma) covalently coupled with 10 μg RC-19 by dimethyl pimelimidate (Pierce, Rockford, IL, USA) was incubated with 15 mg protein overnight at 4°C. The beads were eluted with sample buffer of SDS–polyacrylamide gel electrophoresis (PAGE) for 5 min at 100°C, and reduced with dithiothreitol (DTT). The eluted immunoprecipitant proteins were suspended in 125 mM Tris-HCl buffer (pH 6.8) containing 5 mM 2-mercaptoethanol, SDS and bromophenol blue, and subjected to SDS–PAGE. After protein separation, the gel was stained overnight with 0.1% silver using the silver stain MS kit (Wako, Japan). A silver-stained band of approximately 67 kDa was excised from the gel, de-stained with the de-staining solution of the silver stain kit, and the proteins digested in-gel with trypsin (Izumi *et al.* 2003). Digested peptides were extracted from gel pieces with 50 μL 50% acetonitrile and 0.1% trifluoroacetic acid. A C18 microcolumn (Millipore) was used for purification of peptides. A matrix-assisted laser resorption ionization (MALDI) time-of-flight (TOF) mass spectrometer (Bruker Daltonics, USA) was used to detect ERα protein directly. Samples were prepared by mixing 0.5 μL peptide solution with 0.5 μL matrix solution on a MALDI plate. All masses are reported as monoisotopic mass values. Peptides were identified using the Mascot search program (http://www.matrixscience.com) to perform theoretical trypsin digests, and to search for potential unmodified tryptic peptides (with up to one missed cleavages) or suspected modified species. Further details are described in Supplementary material.

RT-PCR and Southern hybridization

Total RNAs were isolated from rat brain tissues using a total RNA purification kit (Nippongene, Japan) (Furukawa *et al.* 1998). The purified RNAs were quantified on the basis of absorbance at 260 nm, and then treated with RNase-free DNase I to eliminate the possibility of genomic DNA contamination. RNA was reverse-transcribed, using a T-primed first-strand kit (Pharmacia, Sweden). Specific primer pairs for subregions of ERα exons (Exon 1′-2-3-4′, Exon 3′-4-5′, Exon 4′-5-6′, Exon 5′-6-7′ and Exon 6′-7-8′), and their distribution along exons, are illustrated in Fig. S6 in Supplementary material. Specific primer sequences of ERβ (Exon 7′-8′) and the PCR protocol for both molecules are described in Supplementary material. Exon 3′-4-5′ primer pairs of ERα were used for semi-quantitative analysis performed for comparison of several brain regions and developmental analysis (Ivanova and Beyer 2000). To achieve specific detection of mRNAs, we chose primer pairs which had Gibb's free energy around − 8 kcal/mol (forward five bases) and − 9 kcal/mol (backward five bases) upon recombination with cDNA. The amplified RT-PCR products were directly cloned into TA-cloning vector (Promega, Madison, WI, USA), sequenced, and used as DNA probes of the following Southern hybridization. The RT-PCR products were separated on 1.8% agarose gels, stained with ethidium bromide and then transferred to nylon membranes. Southern hybridization was performed with ^{32}P-labeled cDNA probes for ERα. The hybridization signals were measured using a BAS-1000 Image analyzer (Fuji film, Japan). Four independent analyses produced identical results. In addition to ethidium bromide staining, cloning of cDNA and Southern hybridization were used to ensure the detection of target cDNA.

Results

Rapid effect of estradiol on long-term depression (LTD)

We carried out electrophysiological investigations to analyze the effect of 17β-estradiol on LTD. LTD was simultaneously investigated in CA1, CA3 and DG of the same adult male hippocampal slices. Recordings were performed using novel 64 multi-electrodes particularly arranged to stimulate the Schaffer collaterals in the stratum radiatum of CA1, the recurrent collateral fibers in the stratum radiatum of CA3 and the medial perforant pathways in the molecular layer of DG (Fig. S1). LTD was induced pharmacologically by the transient application (3 min) of NMDA. Upon application of 30 μM NMDA, the maximal amplitude of EPSP was transiently decreased to a minimal value, and then recovered to reach an approximate plateau level (< 100%) within 30–50 min after NMDA application, indicating LTD establishment (Fig. 1a). This LTD was induced by the activation of phosphatase due to a moderate Ca^{2+} influx through NMDA receptors (Lee *et al.* 1998). The plateau EPSP amplitude at 60 min was 80.4% (CA1), 88.8% (CA3) and 95.1% (DG). A 30 min pre-perfusion of 10 nM estradiol, for example, significantly enhanced LTD, resulting in the EPSP amplitude at 60 min of 59.7% (CA1), 79.1% (CA3) and 92.2% (DG) (Fig. 1a). The dose dependency of the enhancement effect by 17β-estradiol was heterogeneous in different regions. LTD enhancement was least significant at 0.1 nM, moderately significant at 1 nM and most significant at 10 nM for 17β-estradiol in both CA1 and CA3. In DG, however, LTD enhancement was most significant at 1 nM, and a smaller enhancement was observed at 0.1 nM and 10 nM for estradiol. Investigations using specific estrogen agonists indicated that the contribution of ERα (but not ERβ) was essential to these estradiol effects. PPT (ERα agonist) at 100 nM exhibited a significant LTD enhancement in CA1 (Figs 1b and c), while DPN (ERβ agonist) did induce a suppression of LTD in CA1 (Fig. 1c), suggesting a contribution of ERβ opposite to that of ERα in the observed estradiol effect on LTD.

The co-perfusion of 10 nM 17α-estradiol (used as an antagonist) with 1 nM 17β-estradiol suppressed the 17β-estradiol effect on LTD. The co-perfusion of 1 microM ICI with 10 nM 17β-estradiol, however, did not block the 17β-estradiol-induced enhancement of LTD. DES at 1–10 nM enhanced LTD, and DES was more effective at

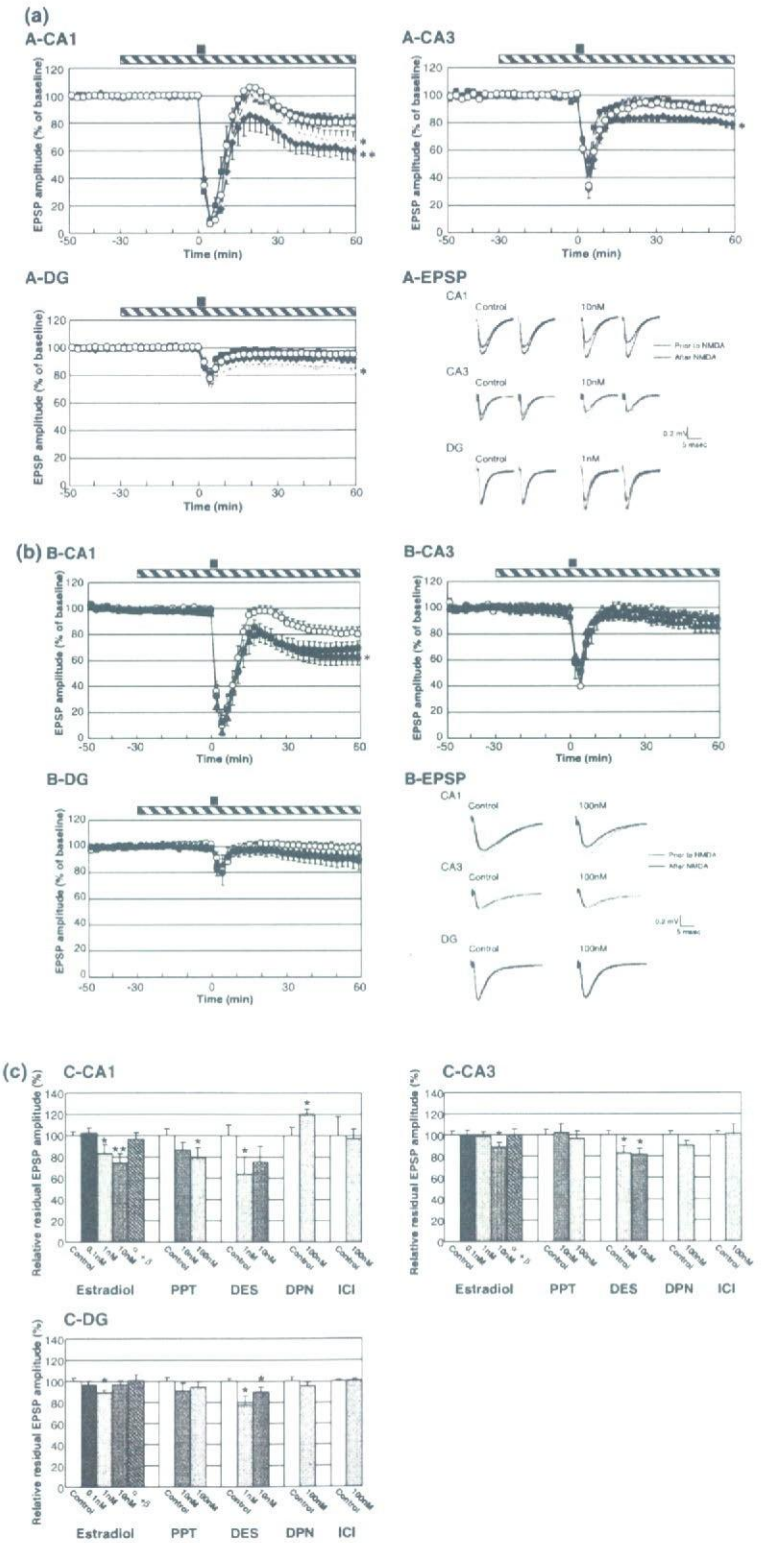

Fig. 1 (a) Rapid modulation by 17β-estradiol of LTD in the CA1 (A-CA1), CA3 (A-CA3) and DG (A-DG) of the same hippocampal slice. Estradiol concentration was 0 nM (open circle, $n = 17$) and 0.1 nM (blue filled square, $n = 8$), 1 nM (yellow filled triangle, $n = 11$) and 10 nM (red filled diamond, $n = 10$), respectively; n = number of independent experiments. Vertical axis indicates maximal amplitude of EPSP. Here, 100% refers to the EPSP value at t = − 40 min prior to NMDA stimulation, irrespective of the test condition. LTD was induced by 30 μM NMDA perfusion at time t = 0–3 min (filled bar above the graph). Hatched bar above the graph indicates period of time during which estradiol was administered. The significance of the estradiol effect was confirmed at 60 min via statistical analysis using ANOVA ($^*p < 0.05$; $^{**}p < 0.01$) as indicated in the figure. Illustrated data points and error bars represent the mean ± SEM from n independent slices. A-EPSP = EPSP traces in the presence of 10 nM estradiol, showing sample recordings taken prior to (t = − 40 min) and after (t = 60 min) NMDA stimulation. (b) Rapid modulation by PPT of LTD in the CA1 (B-CA1), CA3 (B-CA3) and DG (B-DG) of the same hippocampal slice. PPT concentration was 0 nM (open circle, $n = 10$), 10 nM (blue filled square, $n = 8$) and 100 nM (red filled triangle, $n = 12$), respectively. B-EPSP = EPSP traces in the presence of 100 nM PPT, showing sample recordings taken prior to and after NMDA stimulation. (c) Comparison of modulation effect of LTD by 17β-estradiol and agonists in the CA1, CA3 and DG of hippocampal slices. Vertical axis is relative EPSP amplitude at t = 60 min, where EPSP amplitude at t = 60 min of the control slice without drug application is taken as 100%. From left to right, 17β-estradiol (Estradiol), PPT, DES, DPN and ICI at indicated concentrations. In Estradiol, α + β indicates that 10 nM 17α-estradiol was perfused with 1 nM 17β-estradiol. The significance of the estradiol effect was confirmed at 60 min via statistical analysis using ANOVA ($^*p < 0.05$; $^{**}p < 0.01$) as indicated in the figure.

1 nM than 10 nM. The GPR30 agonist, 100 nM ICI, did not affect the NMDA-induced LTD. In Fig. 1(c), a quantitative comparison was shown by normalizing the EPSP value of the control LTD curve at 60 min to 100%. This normalization was performed for all pairs of control and drug-treated slices because the control LTD responses varied slightly between different drug treatment pairs, depending on differences in the animals. Here, we investigated LTD in particular because LTD has not been extensively analyzed compared with long-term potentiation. The comparison between three subregions indicated that estradiol modulation of LTD is more effective in CA1 than in CA3 and DG. The enhancing effect of LTD by estradiol suggests that estradiol could facilitate erasing processes of memory. Because the baseline EPSP was stable during the 120 min estradiol perfusion (in the case of absence of NMDA application), newly-generated spines (see below) during the 120 min incubation with estradiol probably did not form active synapses that contribute EPSP and LTD signals.

Rapid effect of estradiol on spinogenesis

Next, we analyzed the ability of 17β-estradiol to modulate spine density and morphology. To do this, single spine imaging was performed for Lucifer Yellow-injected neurons in hippocampal slices from 12-week-old male rats. These investigations were independent of synaptic transmission investigations such as LTD and LTP, which probe the characteristics of pre-formed synapses. The single spine imaging not only probes pre-existing spines but also, newly-formed spines upon estradiol treatment. The spinogenesis investigations also analyzed both spine synapses (spines forming synapses) and free spines (spines without forming synapses), whereas in the LTD measurements we obtained information about a particular population of spines that form synapses (spine-synapse). As we found the greatest modulation effect of estradiol in CA1 in the LTD experiments, we focus here on CA1 neurons for analysis of spinogenesis. It should be noted that the analysis of spinogenesis in CA3 has been reported elsewhere (Tsurugizawa *et al.* 2005).

We analyzed secondary branches of the apical dendrites located 150–250 μm distant from the pyramidal cell body around the middle of the stratum radiatum of CA1 region. Following a 0.5–2 h treatment with 17β-estradiol, treated dendrites have significantly more spines than control dendrites (i.e. with no estradiol). Time dependency was examined by treating slices for 0.5, 1 and 2 h with 1 nM estradiol. The enhancing effect on the total spine density was approximately proportional to the incubation time, showing 1.05 (0.5 h), 1.13 (1 h) and 1.31 spines/μm (2 h). Dose dependency was also examined after a 2 h incubation, and showed that the enhancing effect was most significant at 1 nM estradiol (1.31 spines/μm) compared with 0.1 nM (1.03 spines/μm) and 10 nM (1.25 spines/μm) estradiol. Because a 2 h treatment with 1 nM estradiol was most effective for spinogenesis, this incubation time was used in the following investigations unless specified. The different contributions of ERα, ERβ and GPR30 in the effect of estrogen can be investigated using the ERα-specific agonist, PPT, the ERβ-specific agonist, DPN (Harrington *et al.* 2003) and the GPR30-specific agonist, ICI (Thomas *et al.* 2005).

A 2 h treatment increased the total spine density to 1.31 spines/μm (1 nM estradiol) compared with 0.85 spines/μm (control, 0 nM estradiol) (Figs 2a and b). PPT (Harrington *et al.* 2003) at 100 nM induced a significant enhancement of spine density to 1.20 spines/μm (Fig. 2b). However, DPN (Harrington *et al.* 2003) at 100 nM increased the spine density only slightly (0.95 spines/μm). Diethylstylbestrol (DES, agonist of ERα and ERβ) significantly increased spine density. A stronger effect was observed for 1 nM DES (1.29 spines/μm) than 10 nM DES (0.99 spines/μm). Blocking of ERα by 1 μM ICI 182,780 and of NMDA receptors by MK-801 completely suppressed the enhancing effect of estradiol on spine density. Blocking phosphorylation of mitogen-activated protein (MAP) kinase by 50 μM PD98059 completely prevented estradiol-induced spinogenesis. Blocking Src kinase by PP2 did not significantly suppress the estradiol effect. Blocking of AMPA receptors by CNQX at 20 μM only partially prevented the estradiol-enhancing effect by decreasing spine density to 1.07 spines/μm. Washout of estradiol for an additional 2 h after the 2 h estradiol treatment abolished the estradiol-induced enhancement of spinogenesis, implying that these action are reversible. The specific ligand of GPR30, 100 nM ICI and tamoxifen (Thomas *et al.* 2005), did not significantly increase spine density (Fig. 2b).

The morphological changes in spines induced by 2 h drug treatments were quantitatively assessed (Figs 2d,e). In the control slices (0 nM estradiol), the relative population of spines was approximately 24% for mushroom spines, 62% for thin spines, 1% for filopodia and 13% for stubby spines (Fig. 2c). Upon estradiol treatment, the densities of thin spines and filopodia were increased significantly, from 0.57 spines/μm and 0.01 spines/μm to 0.97 spines/μm and 0.11 spines/μm, respectively, while the densities of mushroom spines (from 0.16 to 0.12 spines/μm) and stubby spines (from 0.10 to 0.11 spines/μm) were not significantly altered within experimental error (Fig. 2d). As a result, the average spine diameter became significantly smaller following estradiol application (Fig. 2e). PPT induced a change nearly identical to that obtained with estradiol. Blocking by PD98059, ICI and MK-801 completely suppressed the enhancing effect of estradiol on the density of thin spines (Fig. 2d).

We estimated the population of spine-synapses that are spines forming synapses. In control slices, approximately 47.3 ± 9.8% of total spines, 61.8 ± 12.7% of mushroom spines, 45.2 ± 9.2% of thin spines, 0% of stubby spines and

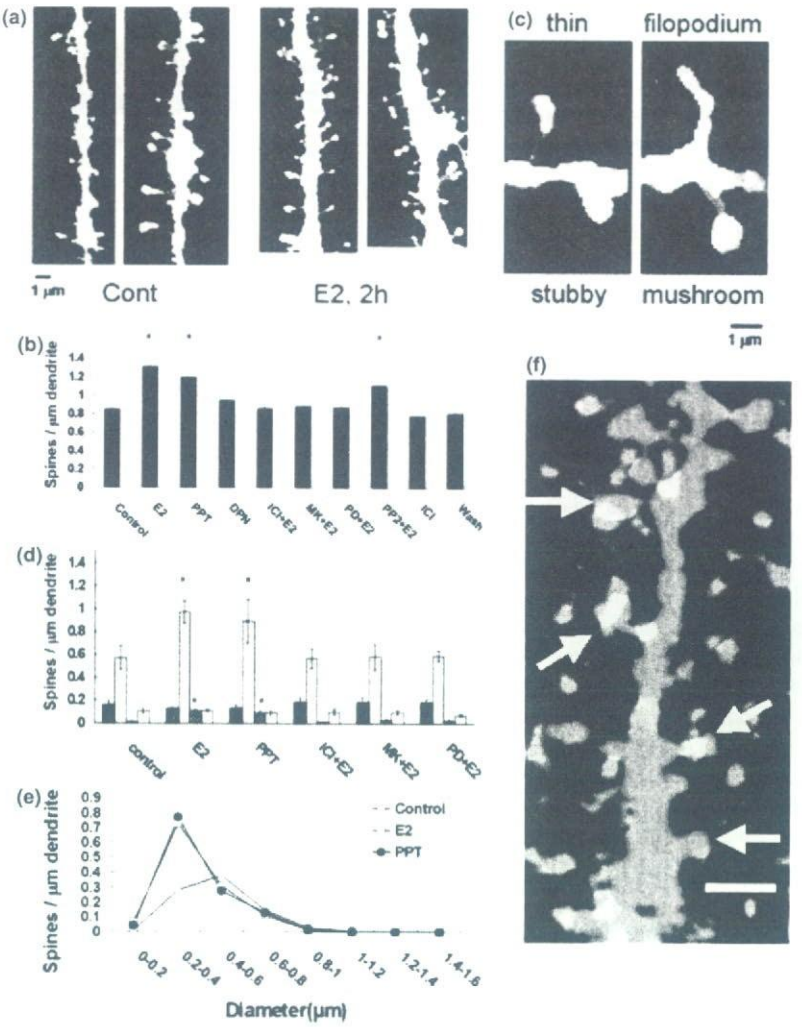

Fig. 2 Changes in the density and morphology of spines upon treatment with 17β-estradiol (E2) and drugs in hippocampal slices. Spines were analyzed along the secondary dendrites of pyramidal neurons in the stratum radiatum of CA1. (a) Maximal intensity projections onto XY plane from z-series confocal micrographs, showing spines along the secondary dendrites of hippocampal CA1 pyramidal neurons. Control spines without drug treatments (Cont) and spines after E2 treatment (E2). Bar = 1 μm. (b) Effect of drug treatments on the total spine density in CA1 neurons. Vertical axis is the average number of spines/1 μm. A 2 h treatment in ACSF without drugs (Control), or with 1 nM E2 (E2), 100 nM PPT (PPT), 100 nM DPN (DPN), 1 nM E2 and 1 μM ICI 182,780 (ICI + E2), 1 nM E2 and 50 μM MK-801 (MK + E2), 1 nM E2 and 50 μM PD98059 (PD + E2), 1 nM E2 and 25 μM PP2 (PP2 + E2), 100 nM ICI (ICI) or 1 nM E2, followed by 2 h washout with ACSF (Wash). (c) Four different spine subtypes are shown: mushroom type, thin type, filopodium type and stubby type. Bar = 1 μm. (d) Density of four subtypes of spines. A 2 h treatment in ACSF without drugs (Control group), or with 1 nM E2 (E2 group), 1 nM E2 and 1 μM ICI (ICI + E2 group), or 1 nM E2 and 50 μM MK-801 (MK + E2 group). In each group, from left to right: mushroom (black column), thin (dotted column), filopodium (hatched column) and stubby (open column). (e) Histogram of spine head diameters after a 2 h treatment in ACSF without drugs (Control, open circle), or with 1 nM E2 (open square) and 100 nM PPT (filled circle). (f) Distribution of spine-synapses in slices. Synapse formation is indicated as yellow regions that are superimposed regions of spines visualized with Lucifer Yellow (green) on axon terminals stained with anti-synapsin I IgG (red). Spine-synapses are indicated by arrows. Other yellow regions may be shaft-synapses, which are synaptic contacts ending directly on the dendrite. Lucifer Yellow was injected into a single neuron in a slice (400 μm thick), then the slice was further frozen-sliced (30 μm thick) and immunostained with anti-synapsin I IgG (1/500). Distribution of secondary antibody conjugated with Cy3 was analyzed by confocal microscopy. Scale bar = 2 μm. In (b), (d) and (e), results are reported as mean ± SEM from $n = 11$ (control) or $n = 5$ (drug-treated) different neurons, and for each neuron 150–300 spines were analyzed. The significance of the drug effects was confirmed via statistical analysis using ANOVA ($^*p < 0.05$) between control and drug-treated samples as indicated in the figure. In (b), (d) and (e), vertical axis is the average number of spines/1 μm of dendrite.

0% of filopodia were observed to form synapses, as judged from the superimposed region of immunostaining with synapsin I (presynaptic marker) on Lucifer Yellow-injected spines ($n = 5$ neurons, approximately 100 spines) (Fig. 2f). The rest of the spines were free spines without partners of axon terminals.

Western blot analysis of ERα in synaptic and nuclear fractions

Because the 67 kDa ERα protein is present in extremely low levels in the brain relative to the ovary, non-specific IgGs contained in the antisera used in histochemical investigations may result in serious non-specific binding, producing misleading results. Accordingly, the specific reactivity of ERα antibodies should be carefully tested via western immunoblot analysis. We therefore used a novel affinity column-purified RC-19 antibody raised against the 19 C-terminal residues of rat ERα. RC-19 was used as a type of purified MC-20. We also performed careful purification of synaptic membranes, cytoplasm and nuclei using a combination of density gradient centrifugations for the hippocampus and hypothalamus from adult 12-week-old male rats. Using RC-19 (1/2000 dilution), only a single protein band was observed, with a molecular mass of approximately 67 kDa, in the PSD and cytoplasmic fractions as well as the nuclear fraction (Fig. 3a). As a positive control, the 67 kDa band was stained for rat ERα protein expressed in COS-7 cells and ovary from a 4-week-old female rat. The excellent quality of RC-19 was demonstrated by the absence of immunoreactivity in the vicinity of 67 kDa for the hippocampus and hypothalamus from 8-week-old ERα knockout (ERαKO) mice, used as a negative control (Fig. 3c). Extended analysis indicated that ERα was certainly localized in the purified PSD fraction, which was characterized by PSD-95 (Fig. 3b). It should be noted that MAP kinase and Src kinase were both observed in the PSD fraction. ERα was observed in the presynaptic membrane-rich fraction (PRE, low density synaptic membrane fraction, characterized by synaptophysin) and in the cytoplasmic fraction (CYT). The integrated total amount of ERα was greater in the CYT fraction than in other PSD and PRE fractions. It should be noted that the densest band of ERα that appeared in the PSD fraction (Fig. 3b) was simply due to the application of a threefold excess amount of protein in PSD compared with CYT and PRE. The 67 kDa band was not observed when RC-19 antibody was pre-adsorbed with ERα antigen peptides (30 μg/mL).

Western blot with other antisera

For comparison, the reactivity was examined for other antisera widely used in earlier studies. Unfortunately, these antisera failed to react primarily with the 67 kDa ERα protein in the hippocampus. When MC-20 (antiserum against the most C-terminal 20 amino acids of mouse ERα) or

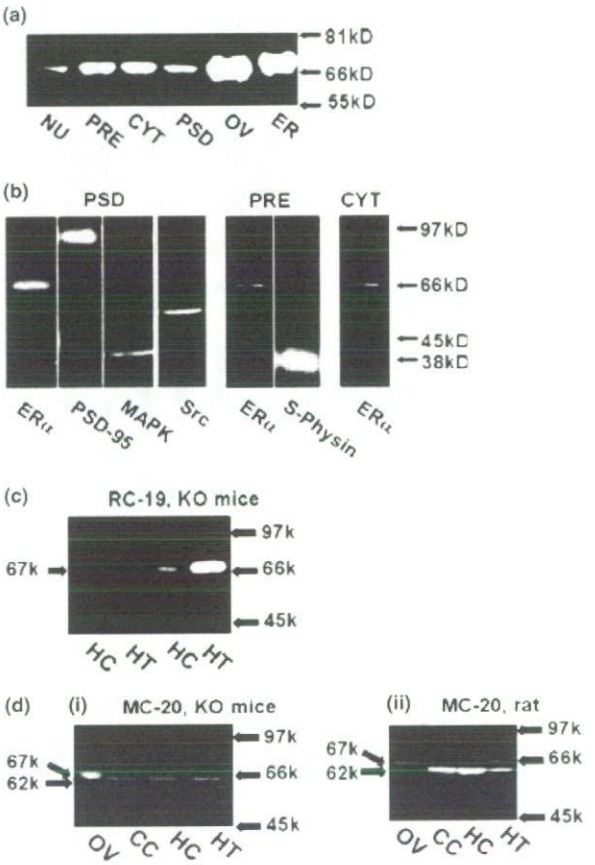

Fig. 3 Western immunoblot of ERα in subcellular fractions of male rat hippocampus. (a) Blot with RC-19 antibody of the subcellular fractions from adult rat hippocampus. From left to right: the nuclear fraction (NU), presynaptic membrane-rich fraction (PRE), cytoplasmic fraction (CYT), postsynaptic density fraction (PSD), ovary (OV) and ERα expressed in COS-7 cells (ER). The amount of protein applied to the gels was 20 μg for each hippocampal fraction, and 1 μg for ERα-expressed COS-7 cells and ovary. Ovary was taken from a 4-week-old rat. ERα genetically expressed in COS-7 was used as a positive control. (b) Western blot of PSD, PRE and CYT of the hippocampus. From left to middle, blot of PSD with RC-19 IgG (ERα), PSD-95 IgG (PSD-95), MAP kinase IgG (MAPK) and Src IgG (Src). From middle to right, blot of PRE with RC-19 (ERα) and synaptophysin IgG (S-Physin). At rightmost lane, blot of CYT with RC-19 (ERα). It should be noted that the amount of protein applied was 20 μg for each lane, but 60 μg for the PSD fraction. The densest staining of ERα was therefore shown in PSD, although the staining of ERα in PSD was weaker than that in the CYT and PRE fractions. (c) Staining with RC-19 of tissue homogenates from ERαKO mice and wild mice. From left to right, hippocampus (HC) and hypothalamus (HT) from ERαKO mice, HC and HT from wild mice. (di) Staining with MC-20 antiserum of tissue homogenates from adult ERαKO mice brain. From left to right, ovary (OV, 4-week-old rat), cerebral cortex (CC), HC and HT. (dii) Staining with MC-20 antiserum of tissue homogenates from adult male rat brain. From left to right, OV from rat, CC, HC and HT. The amount of protein applied to the gels was 20 μg for each lane in panels (c) and (d).

AS409 (polyclonal antiserum against rat ERα expressed in *Escherichia coli*) (Weiland *et al.* 1997) was used, the molecular weights of the main immunoreactive bands were different from 67 kDa. Genetically-expressed ERα or ovary was used as a control to differentiate 67 kDa from 62 kDa. MC-20 (1/3000) yielded a very weak 67 kDa band and a major, approximately 62 kDa band (Fig. 3d) (Toran-Allerand *et al.* 2002), whereas AS409 (1: 2000) gave a weak 67 kDa band and a major, approximately 90 kDa band (Fig. S3 in Supplementary material). Note that MC-20 also demonstrated a significant reactivity with a 62 kDa band in the hippocampus of ERαKO mice (Fig. 3d).

In the ERαKO mice (exon 2 deleted ERα-Δ2 KO) used in this study, no ERα RNA containing transcripts of any of the exons located downstream of exon 2 was detected by RT-PCR, implying that this 62 kDa protein could not be a splice variant of ERα (Dupont *et al.* 2000; Pendaries *et al.* 2002). Our ERαKO mice are essentially different from ERα-Neo KO mice (constructed by Neomycin insertion into exon 1) that have expressed an ERα splice variant, i.e. N-terminal modified ERα (61 kDa) (Couse *et al.* 1995; Kos *et al.* 2002).

Western blot examination for RC-19, MC-20 and AS409 has shown that the use of antibody purified from antiserum is essential to obtain real staining of ERα in the hippocampus.

Immunohistochemistry of ERα in hippocampal principal neurons

Immunohistochemical staining of ERα proteins via column-purified RC-19 antibodies (1/1000) was performed to determine the cell-specific localization of ERα in the adult male rat hippocampus. An intense immunoreactivity was observed in extranuclear, as well as nuclear regions of principal neurons in the CA1–CA3 and the dentate gyrus (DG) regions (Fig. 4a). Pre-adsorption of the antibody with an excess of ERα antigen (30 μg/mL) resulted in the

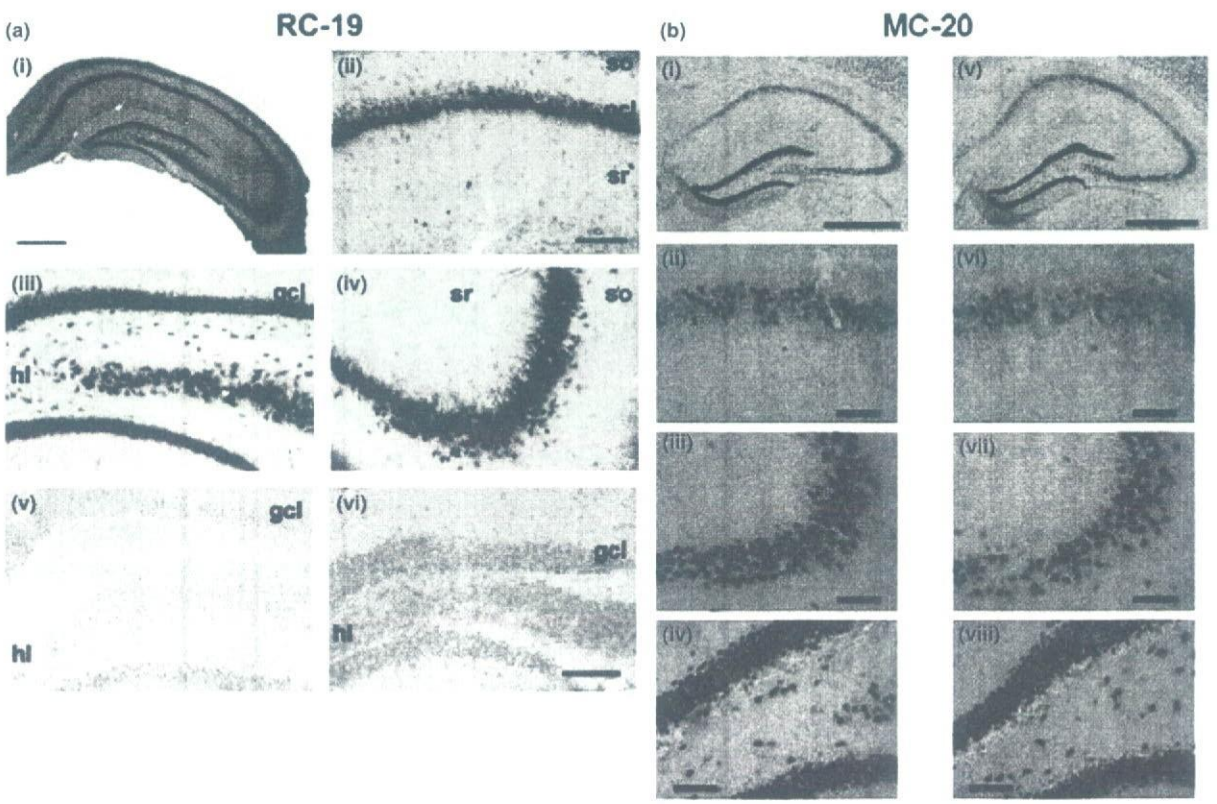

Fig. 4 (a) Immunohistochemical staining of ERα with RC-19 antibody in the hippocampal slices of adult male rat (i–v) and adult ERαKO mouse (vi). (i) Coronal section of the whole hippocampal formation; (ii) CA1; (iii) DG; (iv) CA3; (v) DG incubated with RC-19 antibody pre-adsorbed with antigen of C-terminal 19 amino acids of ERα; (vi) the DG of ERαKO mouse. Abbreviations: so, stratum oriens; pcl, pyramidal cell layer; sr, stratum radiatum; gcl, granule cell layer; hl, hilus. Scale bar = 500 μm in (i) and 200 μm in (ii)–(vi). Several independent experiments were performed. (b) Immunohistochemical staining with MC-20 antiserum in the hippocampal slices of adult ERαKO (i–iv) and wild male mice (v–viii): (i), (v) coronal section of the whole hippocampal formation; (ii), (vi) CA1 region; (iii), (vii) CA3 region; (iv), (viii) dentate gyrus. Scale bar = 50 μm for (i) and (v); 10 μm for (ii–iv) and (vi–viii). Three different batches of MC-20 were used.

complete disappearance of immunoreactivity in the hippocampus. No positive immunoreactivity was obtained using RC-19 in the hippocampus from ERαKO mouse (Fig. 4a). MC-20 (1/500) without purification, on the other hand, showed a significant reactivity for principal neurons in the hippocampal slices from ERαKO mouse (Fig. 4b) as well as from adult male rat (Fig. S4 in Supplementary material). Here, three independent batches of MC-20 showed nearly identical results. Note that RC-19 immunoreactivity was not observed in glial-like cells from immunohistochemical and immunogold investigations, excluding a significant contribution of glial cells.

Ultrastructural analysis for synaptic and nuclear localization of ERα

To explain the site of rapid modulation of spinogenesis and LTD of glutamatergic neurons by the activation of ERα, clarification of subcellular localization (particularly synaptic localization) of ERα in glutamatergic neurons is essential. The extranuclear and nuclear localization of ERα was clarified via ultrastructural investigations using RC-19 (1/1000). An immunoelectron microscopic analysis using post-embedded immunogold was performed to determine the localization of ERα immunoreactivity in the hippocampal neurons of adult male rats. ERα was localized not only in the nuclei but also, in both the axon terminals and dendritic spines of principal neurons (Fig. 5, Fig. S5 in Supplementary material). Gold particles were clustered in the postsynaptic and presynaptic compartments, as well as in the nuclei, dendrites and cytoplasm. At postsynapses, gold particles were distributed within the cytoplasm of the spine head. In some cases, gold particles were affiliated within the postsynaptic density. Significant labeling along dendrites was also found (Fig. 5), although many fewer gold particles were observed in axons. In glial-like cells, gold particles were not clearly recognized. Multiple labeling (three or more) of immunogold in the pre- and postsynaptic compartments was confirmed to ensure the specific labeling. A search for immunogold-labeled ERα proteins was performed for at least 30 synapses for each CA1, CA3 and DG region from more than 100 independent images. Almost no mitochondrial labeling was observed, indicating very low background nonspecific labeling as RC-19 did not recognize the ERα band in the mitochondria by western blot. The topological distributions of gold particles within the neurons of the CA1, CA3 and DG were essentially identical. Pre-adsorption of the antibody with ERα antigen (30 μg/mL) resulted in the disappearance of immunoreactivity. MC-20 immunoreactivity was strong in synapses and MC-20 (1/2000) often stained synaptic mitochondria (Fig. S5). These results raised some doubts about the staining specificity of MC-20. It should be noted that to date, ultrastructural investigations have suggested the presence of ERα mainly in GABAergic interneurons and cholinergic neurons using AS409 antiserum (Milner *et al.* 2001; Adams *et al.* 2002; Towart *et al.* 2003), with one report showing ERα in pyramidal neurons (Adams *et al.* 2002).

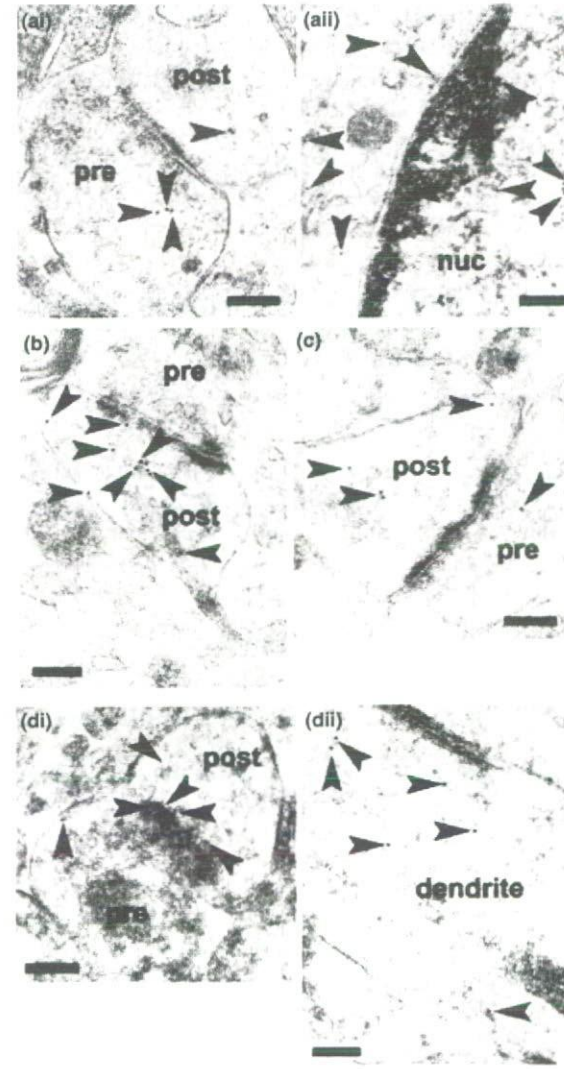

Fig. 5 Immunoelectron microscopic analysis, using RC-19 antibody, of the distribution of ERα within the axospinous synapses and nuclei of the hippocampal principal neurons in the stratum radiatum of CA1 (a), stratum radiatum of CA3 (b) and hilus of DG (c) regions. Representative images are shown from approximately 150 photographs from 32 independent slices from five animals. Gold particles (arrowheads) were localized in the pre- and postsynaptic regions (ai, b and c). In dendritic spines, gold particles were found within the spine head and in some cases, associated with PSD regions (di, axospinous synapses of the hippocampal principal neurons in the stratum radiatum of CA1). Gold particles were also localized in the nuclei (aii). In dendrites, gold particles were often found in the cytoplasmic space (dii, DG region). A 1 : 1000 dilution of RC-19 was used to prevent non-specific labeling. Abbreviations: pre, presynaptic region; post, postsynaptic region; nuc, nucleus. Scale bar = 200 nm.

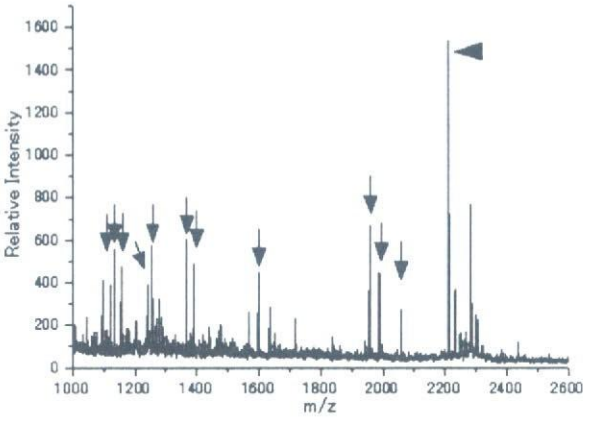

Fig. 6 MALDI-TOF mass spectrum of tryptic peptides from the 67 kDa band obtained after the separation of RC-19 reactive precipitants of the cytoplasmic fractions of hippocampus using SDS–PAGE. Eleven peptides appeared in the spectrum and were attributed to tryptic peptides from ERα as presented in Table 1. The masses matched with tryptic peptides of ERα are indicated by arrows. A large peak at m/z 2211 (arrow head) is the tryptic fragment of trypsin used for validation.

Table 1 Mass spectrometric identification of tryptic peptides from the 67 kDa protein, separated by SDS–PAGE of the RC-19 reacted-precipitants of the cytoplasmic fraction. The observed mass and the corresponding tryptic peptides of ERα are listed with the deviation from the theoretical mass (see Fig. 6)

Observed (m/z)	Deviation	Peptide sequence
1097.41	−0.03	NEMGTSGDMR (283–292)
1122.50	0.01	GMEHLYNMK (526–534)
1132.62	0.0	DHIHRVLDK (478–486)
1240.66	−0.01	ELVHMINWAK (358–367)
1268.73	0.03	INDTLIHLMAK (487–497)
1366.69	0.04	GNMIMESAKETR (177–188)
1389.94	0.05	LAQLLLILSHIR (509–520)
1598.80	−0.01	KCYEVGMMGGIRK (249–262)
1956.10	0.67	SIILLNSGVYTFLSSTLK (455–472)
1987.21	0.0	LAQLLLILSHIRHMSNK (509–525)
2057.91	−0.12	KCYEVGMMKGGIRKDRR (249–265) 2 oxidation (Met)

Mass spectrometric identification of RC-19-reacted ERα

To prove that the RC-19-reactive protein in the above experiments was ERα, mass spectrometric analysis was performed using the cytoplasmic fraction of the hippocampus. RC-19-reactive protein was immunoprecipitated, and an approximately 67 kDa protein was separated by SDS–PAGE. The protein was treated by in-gel protease (trypsin) digestion, and digested peptides were analyzed by MALDI-TOF mass spectrometry. Peptides were identified using the MASCOT search program (Matrix Science). As indicated in Fig. 6, more than 20 tryptic peptides were detected in mass spectrum, and 11 of the major peaks were attributed to the tryptic peptides from ERα. The identified peptides are listed in Table 1. These results strongly suggest that the RC-19-reacted protein is real ERα in the hippocampus.

Analysis of ERα and ERβ mRNA

The possibility of the presence of a splice variant of ERα mRNA, corresponding to the 62 kDa protein detected by MC-20, was excluded in wild-type adult male rat hippocampus using RT-PCR combined with western blot analysis. The potential presence of isoforms of ERα is indicated by the observed reaction of ERα antisera (e.g. MC-20, AS409) with bands of approximately 62 and 90 kDa. ERα is transcribed from eight exons, denoted 1–8. The start and stop codons, corresponding to the ERα N- and C-termini, are included in exons 1 and 8, respectively. Several sets of forward and reverse primer pairs (Fig. S6) were used to examine the transcripts from several distinct subregions of mRNA. No PCR products lacking any of exons 2–7 were observed (Fig. 7). It should be noted that the inclusion of exon 8 was not explicitly examined using RT-PCR because the most C-terminal subregion must be included for western blot-reacted protein with C-terminal antibody RC-19. Although we did not investigate exon 1 deleted form of mRNA, 46 kDa protein should be expressed as reported in uterine tissue (Pendaries *et al.* 2002) in case of the expression of exon 1 deleted splice variant. However, scarcely any 46 kDa protein was observed in the hippocampus and hypothalamus, as judged from western blot with RC-19 (Fig. 3b). The combination of mRNA and western blot analyses therefore demonstrated that splice variants with molecular weights of approximately 62 kDa were not present in the wild-type rat hippocampus. It should be noted that no splice variants of ERα mRNA were expressed in our ERαKO mice (Dupont *et al.* 2000; Pendaries *et al.* 2002).

The expression levels of ERα transcripts in the hippocampus and other brain regions were compared by semi-quantitative RT-PCR using primer pairs designed for the region of exon 3′-4-5′. The relative levels of ERα mRNA expression observed in various brain regions were approximately 1/20 (hippocampus), 1/2 (hypothalamus), 1/15 (cerebral cortex) and 1/80 (cerebellum) compared with levels in the 12-week-old ovary (Fig. S7A in Supplementary material). The relative levels of ERα mRNA transcripts in the hippocampus varied with age, from 100% (post-natal 10-day-old) to approximately 48% (4-week-old) and approximately 56% (adult) for the male rat. In addition, the relative level of ERα mRNA expression was not significantly different between male and female rat hippocampus from investigations of approximately 10 animals. These results were consistent with western blot investigations with RC-19, which also showed almost the same levels of ERα protein in the adult hippocampal homogenates of male and female rats.

The expression levels of ERβ transcripts in the hippocampus and other brain regions were also compared using

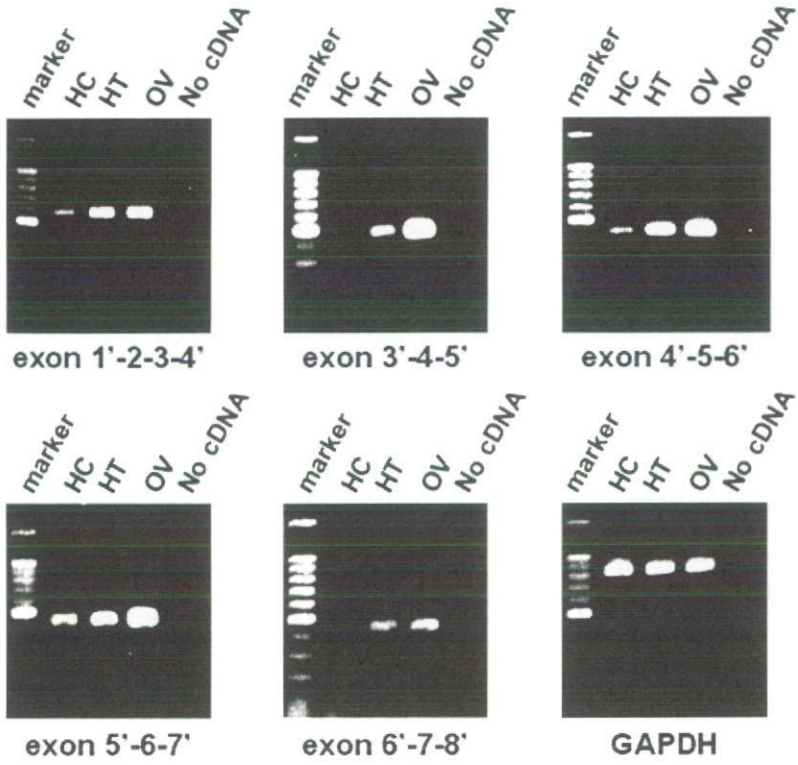

Fig. 7 Investigations regarding the absence of splice variants of ERα mRNA. RT-PCR of mRNA subregions of ERα in the adult rat hippocampus (HC), hypothalamus (HT) and 4-week-old rat ovary (OV). Five subregions were analyzed. Subregion 1′-4′ contained full exons 2 and 3, in addition to partial sequences of nearest exons 1 and 4, as described in the primer pair design (see Supporting information). Subregions 3′-4-5′, 4′-5-6′, 5′-6-7′ and 6′-7-8′ contained full exon 4, exon 5, exon 6 and exon 7, respectively, in addition to partial sequences of the nearest exons. RT-PCR products (each from 50 ng of template) were visualized with ethidium bromide. Left-most lane shows a marker (100 bp ladder); right-most lane is water, used as a negative control.

primer pairs designed for the region of exons 7 and 8. The relative levels of ERβ mRNA expression were approximately 1/80 (hippocampus), 1/20 (hypothalamus), 1/50 (cerebral cortex) and 1/20 (cerebellum) compared with levels in the 12-week-old ovary (Fig. S7B).

The relative expression level of ERα mRNA was approximately 10-fold that of ERβ mRNA in the adult hippocampus, as judged from the PCR cycles needed for ERα (34 cycles) and ERβ (36 cycles) (Figs. S7A and S7B). This level of ERα 10-fold higher than ERβ is in good agreement with the observation that the mode of modulation by estradiol of LTD and spinogenesis is mostly the same as that by the ERα agonist, PPT, and very different from that by the ERβ agonist, DPN.

Discussion

The current study demonstrates, in pyramidal and granule neurons from the acute slices of adult male hippocampus, the postsynaptic localization of ERα, and its modulatory function in rapid synaptic transmission (LTD) and spinogenesis of glutamatergic neurons. These two types of synaptic plasticity reflect, in principle, different processes triggered by estradiol.

Estradiol modulation of LTD occurred only in pre-existent synapses because spines newly generated by estradiol treatments did not form new synapses within 2 h, as judged by no increase in the baseline magnitude of the EPSP signal during 2 h (data not shown). However, estradiol generated new thin spines that served as bases for new spine-synapse formation after, for example, more than 24 h (Pozzo-Miller *et al.* 1999). We used isolated hippocampal slices because we focused on the effect of estradiol on the glutamatergic circuits of the hippocampus. In this sense, the current results have a meaning different from many previous *in vivo* studies that investigated the effect of gonadal estradiol on the hippocampus via serotonergic or cholinergic afferents from the limbic system (Woolley *et al.* 1997; Rudick and Woolley 2000, 2003; Leranth *et al.* 2003; MacLusky *et al.* 2005). Both LTD and spinogenesis are enhanced by either 17β-estradiol or the ERα agonist, PPT. In contrast, application of the ERβ agonist, DPN, resulted in a suppressing effect (LTD) or hardly any enhancing effect (spinogenesis), implying a less significant role for ERβ in estradiol modulation of synaptic plasticity (Szymczak *et al.* 2006). Two different types of synaptic plasticity may therefore be modulated dominantly by ERα in glutamatergic excitatory neurons.

Single spine imaging was used to examine all the dendritic spines. Spine morphological investigations detected not only spine-synapses that form functional synapses but also, dendritic protrusions that do not form synapses. Double-staining investigations with Lucifer Yellow and synapsin I demonstrated that approximately 53% of spines were free spines without synapse formation. Electrophysiological

investigations of synaptic transmission were therefore used to examine, in particular, spine-synapses that form functional synapses. Because the estradiol-induced modulation of spine morphology and LTD appeared so rapidly, in the time range of 1–2 h, the synaptic ERα observed at the postsynaptic density (PSD) and postsynaptic compartment (Figs 3a and b, Fig. 5) probably plays an essential role in driving rapid processes.

Rapid effect of estradiol on synaptic transmission via synaptic ERα

Novel multi-electrode probes covering the CA1, CA3 and DG enabled simultaneous measurements of LTD in both pyramidal and granule neurons. Results demonstrated for the first time that both estradiol and the ERα agonists, PPT and DES, induced rapid modulation of synaptic transmission (Fig. 1). Previous electrophysiological studies have shown the rapid effect of estradiol only on the CA1 region of hippocampal slices (Foy *et al.* 1999), although other hippocampal subregions, CA3 and DG, have not been investigated in comparison with CA1.

Not only LTP but also LTD are necessary for complete memory processing (Migaud *et al.* 1998). In the current study, LTD was chosen to probe the modulation effects of estradiol because estradiol was much more effective on LTD than LTP. When the enhancement of LTP by estradiol was observed in CA1, an immediate increase of approximately 20% was induced upon the onset of estradiol perfusion in the baseline of the EPSP slope. A further approximate 130% increase was induced by high-frequency tetanic stimulation of Schaffer collaterals (Foy *et al.* 1999; Bi *et al.* 2000). However, without this approximate 20% baseline increase in EPSP slope (before the tetanic stimulation), the enhancement by estradiol was not apparent with regard to the pure tetanic stimulation-induced LTP (Ito *et al.* 1999; Kawato 2004; Mukai *et al.* 2006). In other words, the magnitude of tetanic stimulation-induced LTP was nearly the same between the presence and absence of estradiol. On the other hand, in the current LTD enhancement by estradiol, an immediate increase in EPSP by the onset of estradiol perfusion was not induced. The current results are in agreement with previous investigations of LTD. For example, estradiol treatment for 2 days *in vivo* facilitated the induction of LTD in ovariectomized rats (Desmond *et al.* 2000). *In vitro* perfusion of 0.1 nM estradiol (very low concentration) was not effective in modulation of LTD in young adult rat hippocampal slices (Vouimba *et al.* 2000), although 0.1 nM estradiol suppressed LTD in aged rats; this suggests that the response to estradiol may be age-dependent. At estradiol concentrations above 1 nM, we obtained enhancement of LTD (Fig. 1).

Important investigations have been performed by Moss and co-workers using knockdown mice (Gu and Moss 1996; Gu *et al.* 1999). They reported no essential contribution of ERα to estradiol-induced rapid enhancement of the kainate currents of CA1 neurons. This conclusion was based on the very small difference observed in the estradiol effect on kainate currents between wild-type and ERα-Neo KO mice constructed by Neomycin insertion into exon 1 (the previously named exon 2) (Couse *et al.* 1995). It should be noted that in Neomycin insertion ERα-Neo KO mice (practically knockdown mice), N-terminal-modified ERα (61 kDa) is expressed (Couse *et al.* 1995; Kos *et al.* 2002; Pendaries *et al.* 2002). Because the N-terminal-modified ERα has been shown to remain active on estradiol binding and carries genomic processes (Kos *et al.* 2002; Pendaries *et al.* 2002), the participation of ERα in the electrophysiological properties of CA1 cannot be excluded from their investigations.

Woolley and co-workers (Woolley *et al.* 1997; Rudick and Woolley 2000, 2003) reported a series of investigations on the slow disinhibitory action of estradiol on the CA1 pyramidal neurons via interneurons by analyzing dendritic spines, electrophysiological properties and c-Fos responses 24–48 h after *in vivo* estradiol treatment of ovariectomized adult female rats. Increase of dendritic spine density by 22% after estradiol s.c. injection correlates well with an increase in glutamate binding to NMDA receptors and a change in electrophysiological properties (Woolley *et al.* 1997). They also found rapid (2 h) and slow (24 h) expression of c-Fos in CA1 pyramidal neurons induced by estradiol (Rudick and Woolley 2000, 2003). Their explanation is based on the observation that the immunoreactivety of AS409 and MC-20 is located primarily in interneurons (Hart *et al.* 2001; Milner *et al.* 2001).

Rapid and delayed effect of estradiol on spine density and morphology

Spine morphology was demonstrated for the first time to be significantly affected by short (0.5–2 h) estradiol treatments in adult male hippocampus (Fig. 2). The density of thin spines was dramatically increased, although the density of mushroom and stubby spines was not significantly altered. Such a selective modulation of thin spines is certainly a novel observation, and is essential for consideration of the neurogenesis and synaptic plasticity controlled by estrogens. The rapid effects of estradiol may be mediated by a signal transduction pathway via postsynaptic ERα (at the PSD), including MAP kinase but not Src kinase, as further judged from inhibitor analysis (Fig. 2b). Because both ERα and MAP kinase are present in the PSD fraction, an efficient coupling between these two proteins can occur at post-synapses (Fig. 3). The abolition of estradiol-induced spinogenesis, by blocking calcium-permeable NMDA receptors by MK-801 (Fig. 2b), was also observed in investigations of a slow effect (48 h) by *in vivo* estradiol treatment, suggesting the particular correlation of an estradiol signaling pathway with a weak spontaneous Ca^{2+} influx into spines via NMDA

receptors, even in the presence of Mg^{2+} blocking in ACSF (Woolley and McEwen 1994).

It should be noted that spine density is not always increased by the estradiol treatment. In CA3 pyramidal neurons, our recent observation demonstrated that the total density of thorns of thorny excrescences (spine-like postsynaptic structures in CA3), having contacts with mossy fiber terminals originated from granule cells, decreased dramatically to approximately 70% upon a 2 h application of 1 nM estradiol (Tsurugizawa *et al.* 2005). Therefore, the estradiol-induced spinogenesis is highly region-specific and heterogeneous.

There have been several *in vivo* studies on the effect of gonadal steroid supplement on the density of spines of pyramidal cells in the CA1 region. Estrogen supplement in ovariectomized female rats (Gould *et al.* 1990; Woolley *et al.* 1990; Woolley and McEwen 1992; Leranth *et al.* 2000, 2002) and androgens in castrated male rats (Leranth *et al.* 2003) increased the number of CA1 spines, resulting in recovery of spines to the level of the wild type. Morphological changes in spines have also been observed in ovariectomized female mice (Li *et al.* 2004). It should be noted that the mechanisms of estradiol action may be different between *in vivo* and *in vitro* experiments, because indirect effects of estradiol may also occur *in vivo* via cholinergic or serotonergic neurons, projecting to the hippocampus, in addition to the direct influence of estradiol on glutamatergic neurons. Leranth *et al.* (2000) demonstrated that s.c. injection of estradiol modulates the cholinergic or serotonergic neurons that project to the hippocampus from subcortical region, resulting in CA1 spinogenesis of ovariectomized female rats. In addition, ovariectomy, necessary to avoid the contribution of plasma estrogens, may have changed the condition of the cholinergic, serotonergic or glutamatergic neurons so that they were short of estrogens and therefore, estratiol supplement had a significant impact. For more discussion see Supplementary material.

Until the current investigations, acute slices of adult hippocampus had not been extensively investigated with regard to the rapid effect of estradiol on spinogenesis and spine morphology. We selected acute hippocampal slices, as the most intact *in vitro* adult neuron networks, for investigations of the rapid effect of estradiol free from the indirect effect of estradiol on glutamatergic neurons via serotonergic/cholinergic neurons. *In vitro* investigations have been carried out, using mainly neonatal hippocampal slice cultures, focusing on slow (1–4 days) effects of exogenous and endogenous estradiol (Pozzo-Miller *et al.* 1999; Bi *et al.* 2000; Rune *et al.* 2002; Prange-Kiel *et al.* 2006).

On the other hand, there have been a number of *in vivo* studies on the effect of gonadal estradiol supplement on the recovery of the density (not morphology) of spines of pyramidal cells in the CA1 region of ovariectomized female rats. In ovariectomized female rats, circulating estrogen is undetectable and the spine density decreases significantly. The significant effect of gonadal estradiol on the recovery of the density of spines has been demonstrated to be dependent on subcortical efferents, because the surgical transaction of fimbria/fornix, which contains subcortical efferents to the hippocampus, has prevented estradiol-induced spinogenesis. A direct comparison between *in vivo* studies and the current *in vitro* slice study is, in principle, not possible, because *in vivo* studies demonstrate the effect of gonadal estradiol on serotonergic or cholinergic afferents projecting to glutamatergic and GABAergic neurons in the hippocampus in addition to the effect of estradiol on hippocampal intrinsic neurons (Woolley *et al.* 1997; Rudick and Woolley 2000; 2003; Leranth *et al.* 2003; MacLusky *et al.* 2005).

Rapid action of hippocampal-derived estradiol

Hippocampus-derived estradiol should play a key role in the rapid action via synaptic ERα as an intracrine modulator of synaptic plasticity. In the current *in vitro* slice study, the exogenous application of estradiol (1–10 nM) was carried out to elevate rapidly the hippocampal estradiol level from the resting level. Exogenous application of estradiol was used because, until now, the method of rapid elevation of endogenous estradiol concentration via activation of its synthesis pathway had not been established. The concentration of endogenous estradiol is approximately 0.6 nM in the hippocampus in the resting state of neural activity (Hojo *et al.* 2004). In accordance with this, we observed a significant effect on LTD and spinogenesis only at > 1 nM estradiol (Figs 1 and 2). For measurement in a more intrinsic condition, methods for the rapid activation of endogenous synthesis of estradiol should be developed, such as NMDA-induced estradiol synthesis (Kawato *et al.* 2002; Hojo *et al.* 2004), or 1–10 Hz low frequency electric stimulation.

The decrease in endogenous estradiol level also effectively modulates synaptic plasticity. The endogenous estradiol level can be decreased, by inhibiting P450arom activity with letrozole for more than 24 h, using hippocampal slice cultures and cell cultures. The suppression of endogenous estradiol synthesis decreased the spine density in CA1 after 4 days of letrozole treatment (Kretz *et al.* 2004). However, with the letrozole treatment, only the slow estradiol depletion effect can be measured (Prange-Kiel *et al.* 2003; Hojo *et al.* 2004). It is virtually impossible to measure the rapid effect on LTD or spinogenesis in the presence of letrozole because a significant decrease in endogenous estradiol by letrozole cannot be achieved within 1–2 h (time range of LTD and rapid spinogenesis experiments).

Previous uncertainty regarding the distribution of ERα immunoreactivity

The current study demonstrates the critical importance of using purified antibody RC-19 for the target protein 67 kDa

ERα in the hippocampus, where its expression level is extremely low (less than 1/100 relative to levels in the endocrine organs). The specificity of RC-19 was validated by careful western blot analysis, including ERαKO mice, in which no protein reacted with RC-19 in the hippocampus (Figs 3c and 4). Mass spectrometric analysis clearly demonstrated that RC-19 reacted with real ERα (Fig. 6). As judged from the presence of only a single ERα mRNA species, and the observation of the single 67 kDa protein band, the synaptic ERα is concluded to be identical to the classical nuclear ERα observed in the nuclei of hippocampal neurons. The mechanisms of stable ERα binding to the PSD layer (Fig. 3b) should be investigated.

Staining with RC-19, in turn, indicates that antiserum MC-20, after purification, could be an appropriate antibody for ERα in the hippocampus. MC-20, used without purification, significantly reacted with unknown proteins in the hippocampus of ERαKO mice. MC-20 antiserum reacted with the 62 kDa protein in the hippocampus, hypothalamus and cerebral cortex not only from wild-type rats but also from ERαKO mice (Fig. 3d). However, in the ovary, MC-20 did not react with the 62 kDa protein and only reacted with the 67 kDa ERα (Fig. 3dii), suggesting that the 62 kDa protein may be selectively expressed in the brain. These results are consistent with those of Toran-Allerand and co-workers (Toran-Allerand *et al.* 2002), who reported the reaction of MC-20 with an approximately 62 kDa protein in the neocortex of both wild-type and ERαKO mice (Toran-Allerand *et al.* 2002). The 62 kDa band stained by MC-20 in the rat hippocampus cannot be a splice variant of ERα, having the same C-terminal sequence as 67 kDa ERα because MC-20 also stained the 62 kDa band in ERαKO mice (exon 2 deleted type) (Fig. 3d) in which no splice variant of ERα mRNA was expressed (Dupont *et al.* 2000; Pendaries *et al.* 2002). Our RT-PCR analysis, which indicated that the only possible splice variant was 46 kDa and not 62 kDa (see Fig. 7), also supports this conclusion. The assertion that there is a relatively small difference between the 62 kDa and 67 kDa MC-20-reacted bands is supported by the coincidence with the 67 kDa band of genetically-expressed ERα, and the 62 kDa of the hypothalamus in which these two bands always appear in parallel (Fig. 3dii).

The present study indicates that the synaptic plasticity of principal neurons is modulated by ERα expressed in the entire principal neurons, and that the hypothesis of interneuron-mediated estradiol modulation is probably not a main mechanism of the synaptic plasticity of principal neurons. The current ERα staining is a goal of previous attempts of ERα staining that demonstrated overall or partial staining of nuclei and cytoplasm of principal neurons of hippocampal slices using *in situ* hybridization, MC-20 or C1355 antiserum (Cardona-Gomez *et al.* 2000; Solum and Handa 2001; Rune *et al.* 2002).

Acknowledgements

We thank Prof. Shinji Hayashi (Yokohama City University) for his kind gift of AS409 antisera. The development of a custom multielectrode probe was performed as a National Project of 'Disruption of learning and memory by endocrine disrupters as measured with novel multielectrode arrays' in Special Coordinate Funds for Promoting Science and Technology of Ministry of Education, Culture, Sports, Science and Technology, Japan.

Supplementary Material

The following material is available online.

Appendix S1

Figure S1 The arrangement of stimulation electrodes (black circle) and recording electrodes (white circle) on a custom multielectrode probe (dotted line represent pyramidal and granule cell layers).

Figure S2 Schematic illustration for diagram of the spine analysis.

Figure S3 (A) Blot with RC-19 antibody of the nuclear and synaptosomal fractions from adult rat brain. From left to right: homogenates of ovary (OV), nuclear fractions of cerebral cortex (nCC), hippocampus (nHC), hypothalamus (nHT), cerebellum (nCL), synaptosomal fractions of cerebral cortex (sCC), hippocampus (sHC), hypothalamus (sHT), cerebellum (sCL), and ERα expressed in COS-7 cells (ER). (B) Staining with AS409 antiserum of tissue homogenates from adult rat. From left to right, OV from 4 week rat, HC, and HT. Representative blots are shown, but several independent experiments are performed for each blot. Molecular weights (97, 66, 45, 38 kDa) indicated in the figure are taken from molecular weight standard proteins.

Figure S4 Immunohistochemical staining with MC-20 antiserum in the hippocampal slices of adult male rat (A-D). (A) The coronal section of the whole hippocampal formation. (B) CA1 region. (C) dentategyrus. (D) CA3 region. so, stratumoriens; pcl, pyramidal cell layer; sr, stratumradiatum; gcl, granule cell layer; hl, hilus. Scale bar, 500 μm for (A), and 200 μm for (B)-(D).

Figure S5 Immunoelectron microscopic analysis, using RC-19 antibody, of the distribution of ERα within synapse of stratum radiatum of CA3 neuron (A), nucleus of CA3 neuron (B), and nucleus of DG (C) regions. A 1:1000 dilution of RC-19 was used to prevent nonspecific labeling. pre, presynapticregion; post, postsynaptic region. Scale bar, 200 nm. (D) Immunoelectron microscopic analysis, using MC-20 antiserum, of the distribution of antigens of MC-20 in the presynaptic regions, in the stratum radiatum of the hippocampal CA3 region. Heavy staining was observed and several gold particles (arrowheads) were associated with the mitochondria (mito). Scale bar, 200 nm.

Figure S6 The distribution of the following subregions of ERα mRNA amplified with specific primer pairs: Exon1′-2-3-4′, Exon3′-4-5′, Exon4′-5-6′, Exon5′-6-7′, and Exon6′-7-8′.

Figure S7 (A) RT-PCR analysis of mRNAs for ERα expressed in the brain subregions. RT-PCR products for mRNAs (50 ng each) of ERα were electrophoresed on 1.5% agarose gel, and visualized with ethidium bromide. (Top) From left to right, size marker (Marker), ovary diluted at 1/50 (1/50 OV), ovary diluted at 1/500 (1/500 OV), cerebral cortex (CC), hippocampus (HC), hypothalamus (HT), cerebellum (CL), no cDNAs (No cDNA) as a negative control. (Middle) Southern hybridizations. (Bottom) The ethidium bromide

staining of GAPDH. The PCR cycles are 34 cycles. (B) RT-PCR analysis of mRNAs for ERβ expressed in the brain subregions. RT-PCR products for mRNAs (50 ng each) of ERβ were electrophoresed on 1.5% agarose gel, and visualized with ethidium bromide. (Top) From left to right, size marker (Marker), cerebral cortex (CC), hippocampus (HC), thalamus (TL), hypothalamus (HT), cerebellum (CL), no cDNAs (No cDNA) as a negative control, and ovary (OV). (Middle) Southern hybridizations. (Bottom) The ethidium bromide staining of GAPDH. The PCR cycles are 36.

This material is available as part of the online article from http://www.blackwellsynergy.com

References

Adams M. M., Fink S. E., Shah R. A., Janssen W. G., Hayashi S., Milner T. A., McEwen B. S. and Morrison J. H. (2002) Estrogen and aging affect the subcellular distribution of estrogen receptor-alpha in the hippocampus of female rats. *J. Neurosci.* **22**, 3608–3614.

Bi R., Broutman G., Foy M. R., Thompson R. F. and Baudry M. (2000) The tyrosine kinase and mitogen-activated protein kinase pathways mediate multiple effects of estrogen in hippocampus. *Proc. Natl Acad. Sci. USA* **97**, 3602–3607.

Cardona-Gomez G. P., DonCarlos L. and Garcia-Segura L. M. (2000) Insulin-like growth factor I receptors and estrogen receptors colocalize in female rat brain. *Neuroscience* **99**, 751–760.

Cohen R. S., Blomberg F., Berzins K. and Siekevitz P. (1977) The structure of postsynaptic densities isolated from dog cerebral cortex. I. Overall morphology and protein composition. *J. Cell Biol.* **74**, 181–203.

Couse J. F., Curtis S. W., Washburn T. F., Lindzey J., Golding T. S., Lubahn D. B., Smithies O. and Korach K. S. (1995) Analysis of transcription and estrogen insensitivity in the female mouse after targeted disruption of the estrogen receptor gene. *Mol. Endocrinol.* **9**, 1441–1454.

Desmond N. L., Zhang D. X. and Levy W. B. (2000) Estradiol enhances the induction of homosynaptic long-term depression in the CA1 region of the adult, ovariectomized rat. *Neurobiol. Learn. Mem.* **73**, 180–187.

Duan H., Wearne S. L., Morrison J. H. and Hof P. R. (2002) Quantitative analysis of the dendritic morphology of corticocortical projection neurons in the macaque monkey association cortex. *Neuroscience* **114**, 349–359.

Dupont S., Krust A., Gansmuller A., Dierich A., Chambon P. and Mark M. (2000) Effect of single and compound knockouts of estrogen receptors alpha (ERalpha) and beta (ERbeta) on mouse reproductive phenotypes. *Development* **127**, 4277–4291.

Foy M. R., Xu J., Xie X., Brinton R. D., Thompson R. F. and Berger T. W. (1999) 17beta-estradiol enhances NMDA receptor-mediated EPSPs and long-term potentiation. *J. Neurophysiol.* **81**, 925–929.

Furukawa A., Miyatake A., Ohnishi T. and Ichikawa Y. (1998) Steroidogenic acute regulatory protein (StAR) transcripts constitutively expressed in the adult rat central nervous system: colocalization of StAR, cytochrome P-450SCC (CYP XIA1), and 3beta-hydroxysteroid dehydrogenase in the rat brain. *J. Neurochem.* **71**, 2231–2238.

Gould E., Woolley C. S., Frankfurt M. and McEwen B. S. (1990) Gonadal steroids regulate dendritic spine density in hippocampal pyramidal cells in adulthood. *J. Neurosci.* **10**, 1286–1291.

Gu Q. and Moss R. L. (1996) 17 beta-Estradiol potentiates kainate-induced currents via activation of the cAMP cascade. *J. Neurosci.* **16**, 3620–3629.

Gu Q., Korach K. S. and Moss R. L. (1999) Rapid action of 17beta-estradiol on kainate-induced currents in hippocampal neurons lacking intracellular estrogen receptors. *Endocrinology* **140**, 660–666.

Harrington W. R., Sheng S., Barnett D. H., Petz L. N., Katzenellenbogen J. A. and Katzenellenbogen B. S. (2003) Activities of estrogen receptor alpha- and beta-selective ligands at diverse estrogen responsive gene sites mediating transactivation or transrepression. *Mol. Cell Endocrinol.* **206**, 13–22.

Hart S. A., Patton J. D. and Woolley C. S. (2001) Quantitative analysis of ER alpha and GAD colocalization in the hippocampus of the adult female rat. *J. Comp. Neurol.* **440**, 144–155.

Hojo Y., Hattori T. A., Enami T. *et al.* (2004) Adult male rat hippocampus synthesizes estradiol from pregnenolone by cytochromes P45017{alpha} and P450 aromatase localized in neurons. *Proc. Natl Acad. Sci. USA* **101**, 865–870.

Ito K., Skinkle K. L. and Hicks T. P. (1999) Age-dependent, steroid-specific effects of oestrogen on long-term potentiation in rat hippocampal slices. *J. Physiol.* **515**, 209–220.

Ivanova T. and Beyer C. (2000) Ontogenetic expression and sex differences of aromatase and estrogen receptor-alpha/beta mRNA in the mouse hippocampus. *Cell Tissue Res.* **300**, 231–237.

Izumi S., Kaneko H., Yamazaki T., Hirata T. and Kominami S. (2003) Membrane topology of guinea pig cytochrome P450 17 alpha revealed by a combination of chemical modifications and mass spectrometry. *Biochemistry* **42**, 14 663–14 669.

Kawato S. (2004) Endocrine disrupters as disrupters of brain function: a neurosteroid viewpoint. *Environ. Sci.* **11**, 1–14.

Kawato S., Hojo Y. and Kimoto T. (2002) Histological and metabolism analysis of P450 expression in the brain. *Meth. Enzymol.* **357**, 241–249.

Kimoto T., Tsurugizawa T., Ohta Y., Makino J., Tamura H., Hojo Y., Takata N. and Kawato S. (2001) Neurosteroid synthesis by cytochrome p450-containing systems localized in the rat brain hippocampal neurons: *N*-methyl-D-aspartate and calcium-dependent synthesis. *Endocrinology* **142**, 3578–3589.

Kos M., Denger S., Reid G., Korach K. S. and Gannon F. (2002) Down but not out? A novel protein isoform of the estrogen receptor alpha is expressed in the estrogen receptor alpha knockout mouse. *J. Mol. Endocrinol.* **29**, 281–286.

Kretz O., Fester L., Wehrenberg U. *et al.* (2004) Hippocampal synapses depend on hippocampal estrogen synthesis. *J. Neurosci.* **24**, 5913–5921.

Lee H. K., Kameyama K., Huganir R. L. and Bear M. F. (1998) NMDA induces long-term synaptic depression and dephosphorylation of the GluR1 subunit of AMPA receptors in hippocampus. *Neuron* **21**, 1151–1162.

Leranth C., Shanabrough M. and Horvath T. L. (2000) Hormonal regulation of hippocampal spine synapse density involves subcortical mediation. *Neuroscience* **101**, 349–356.

Leranth C., Shanabrough M. and Redmond D. E., Jr (2002) Gonadal hormones are responsible for maintaining the integrity of spine synapses in the CA1 hippocampal subfield of female nonhuman primates. *J. Comp. Neurol.* **447**, 34–42.

Leranth C., Petnehazy O. and MacLusky N. J. (2003) Gonadal hormones affect spine synaptic density in the CA1 hippocampal subfield of male rats. *J. Neurosci.* **23**, 1588–1592.

Li C., Brake W. G., Romeo R. D. *et al.* (2004) Estrogen alters hippocampal dendritic spine shape and enhances synaptic protein immunoreactivity and spatial memory in female mice. *Proc. Natl Acad. Sci. USA* **101**, 2185–2190.

MacLusky N. J., Luine V. N., Hajszan T. and Leranth C. (2005) The 17alpha and 17beta isomers of estradiol both induce rapid spine

synapse formation in the CA1 hippocampal subfield of ovariectomized female rats. *Endocrinology* **146**, 287–293.

McEwen B. (2002) Estrogen actions throughout the brain. *Recent Prog. Horm. Res.* **57**, 357–384.

McEwen B. S. and Alves S. E. (1999) Estrogen actions in the central nervous system. *Endocr. Rev.* **20**, 279–307.

Migaud M., Charlesworth P., Dempster M. *et al.* (1998) Enhanced long-term potentiation and impaired learning in mice with mutant postsynaptic density-95 protein. *Nature* **396**, 433–439.

Milner T. A., McEwen B. S., Hayashi S., Li C. J., Reagan L. P. and Alves S. E. (2001) Ultrastructural evidence that hippocampal alpha estrogen receptors are located at extranuclear sites. *J. Comp. Neurol.* **429**, 355–371.

Mitra S. W., Hoskin E., Yudkovitz J. *et al.* (2003) Immunolocalization of estrogen receptor beta in the mouse brain: comparison with estrogen receptor alpha. *Endocrinology* **144**, 2055–2067.

Mukai H., Takata N., Ishii H. T., Tanabe N., Hojo Y., Furukawa A., Kimoto T. and Kawato S. (2006) Hippocampal synthesis of estrogens and androgens which are paracrine modulators of synaptic plasticity: synaptocrinology. *Neuroscience* **138**, 757–764.

Murphy D. D. and Segal M. (1996) Regulation of dendritic spine density in cultured rat hippocampal neurons by steroid hormones. *J. Neurosci.* **16**, 4059–4068.

Oka H., Shimono K., Ogawa R., Sugihara H. and Taketani M. (1999) A new planar multielectrode array for extracellular recording: application to hippocampal acute slice. *J. Neurosci. Meth.* **93**, 61–67.

Orikasa C., McEwen B. S., Hayashi H., Sakuma Y. and Hayashi S. (2000) Estrogen receptor alpha, but not beta, is expressed in the interneurons of the hippocampus in prepubertal rats: an *in situ* hybridization study. *Brain Res. Dev. Brain Res.* **120**, 245–254.

Pendaries C., Darblade B., Rochaix P., Krust A., Chambon P., Korach K. S., Bayard F. and Arnal J. F. (2002) The AF-1 activation-function of ERalpha may be dispensable to mediate the effect of estradiol on endothelial NO production in mice. *Proc. Natl Acad. Sci. USA* **99**, 2205–2210.

Pozzo-Miller L. D., Inoue T. and Murphy D. D. (1999) Estradiol increases spine density and NMDA-dependent Ca2+ transients in spines of CA1 pyramidal neurons from hippocampal slices. *J. Neurophysiol.* **81**, 1404–1411.

Prange-Kiel J., Wehrenberg U., Jarry H. and Rune G. M. (2003) Para/autocrine regulation of estrogen receptors in hippocampal neurons. *Hippocampus* **13**, 226–234.

Prange-Kiel J., Fester L., Zhou L., Lauke H., Carretero J. and Rune G. M. (2006) Inhibition of hippocampal estrogen synthesis causes region-specific downregulation of synaptic protein expression in hippocampal neurons. *Hippocampus* **16**, 464–471.

Razandi M., Pedram A., Greene G. L. and Levin E. R. (1999) Cell membrane and nuclear estrogen receptors (ERs) originate from a single transcript: studies of ERalpha and ERbeta expressed in Chinese hamster ovary cells. *Mol. Endocrinol.* **13**, 307–319.

Rudick C. N. and Woolley C. S. (2000) Estradiol induces a phasic Fos response in the hippocampal CA1 and CA3 regions of adult female rats. *Hippocampus* **10**, 274–283.

Rudick C. N. and Woolley C. S. (2003) Selective estrogen receptor modulators regulate phasic activation of hippocampal CA1 pyramidal cells by estrogen. *Endocrinology* **144**, 179–187.

Rune G. M., Wehrenberg U., Prange-Kiel J., Zhou L., Adelmann G. and Frotscher M. (2002) Estrogen up-regulates estrogen receptor alpha and synaptophysin in slice cultures of rat hippocampus. *Neuroscience* **113**, 167–175.

Shibuya K., Takata N., Hojo Y. *et al.* (2003) Hippocampal cytochrome P450s synthesize brain neurosteroids which are paracrine neuromodulators of synaptic signal transduction. *Biochim. Biophys. Acta* **1619**, 301–316.

Shimono K., Brucher F., Granger R., Lynch G. and Taketani M. (2000) Origins and distribution of cholinergically induced beta rhythms in hippocampal slices. *J. Neurosci.* **20**, 8462–8473.

Shughrue P. J., Lane M. V. and Merchenthaler I. (1997) Comparative distribution of estrogen receptor-alpha and -beta mRNA in the rat central nervous system. *J. Comp. Neurol.* **388**, 507–525.

Simerly R. B., Chang C., Muramatsu M. and Swanson L. W. (1990) Distribution of androgen and estrogen receptor mRNA-containing cells in the rat brain: an *in situ* hybridization study. *J. Comp. Neurol.* **294**, 76–95.

Solum D. T. and Handa R. J. (2001) Localization of estrogen receptor alpha (ER alpha) in pyramidal neurons of the developing rat hippocampus. *Brain Res. Dev. Brain Res.* **128**, 165–175.

Sorra K. E. and Harris K. M. (2000) Overview on the structure, composition, function, development, and plasticity of hippocampal dendritic spines. *Hippocampus* **10**, 501–511.

Szymczak S., Kalita K., Jaworski J., Mioduszewska B., Savonenko A., Markowska A., Merchenthaler I. and Kaczmarek L. (2006) Increased estrogen receptor beta expression correlates with decreased spine formation in the rat hippocampus. *Hippocampus* **16**, 453–463.

Thomas P., Pang Y., Filardo E. J. and Dong J. (2005) Identity of an estrogen membrane receptor coupled to a G protein in human breast cancer cells. *Endocrinology* **146**, 624–632.

Toran-Allerand C. D., Guan X., MacLusky N. J., Horvath T. L., Diano S., Singh M., Connolly E. S., Jr, Nethrapalli I. S. and Tinnikov A. A. (2002) ER-X: a novel, plasma membrane-associated, putative estrogen receptor that is regulated during development and after ischemic brain injury. *J. Neurosci.* **22**, 8391–8401.

Towart L. A., Alves S. E., Znamensky V., Hayashi S., McEwen B. S. and Milner T. A. (2003) Subcellular relationships between cholinergic terminals and estrogen receptor-alpha in the dorsal hippocampus. *J. Comp. Neurol.* **463**, 390–401.

Tsurugizawa T., Mukai H., Tanabe N. *et al.* (2005) Estrogen induces rapid decrease in dendritic thorns of CA3 pyramidal neurons in adult male rat hippocampus. *Biochem. Biophys. Res. Commun.* **337**, 1345–1352.

Vouimba R. M., Foy M. R., Foy J. G. and Thompson R. F. (2000) 17beta-estradiol suppresses expression of long-term depression in aged rats. *Brain Res. Bull.* **53**, 783–787.

Weiland N. G., Orikasa C., Hayashi S. and McEwen B. S. (1997) Distribution and hormone regulation of estrogen receptor immunoreactive cells in the hippocampus of male and female rats. *J. Comp. Neurol.* **388**, 603–612.

Woolley C. S. and McEwen B. S. (1992) Estradiol mediates fluctuation in hippocampal synapse density during the estrous cycle in the adult rat. *J. Neurosci.* **12**, 2549–2554.

Woolley C. S. and McEwen B. S. (1994) Estradiol regulates hippocampal dendritic spine density via an *N*-methyl-D-aspartate receptor-dependent mechanism. *J. Neurosci.* **14**, 7680–7687.

Woolley C. S., Gould E., Frankfurt M. and McEwen B. S. (1990) Naturally occurring fluctuation in dendritic spine density on adult hippocampal pyramidal neurons. *J. Neurosci.* **10**, 4035–4039.

Woolley C. S., Weiland N. G., McEwen B. S. and Schwartzkroin P. A. (1997) Estradiol increases the sensitivity of hippocampal CA1 pyramidal cells to NMDA receptor-mediated synaptic input: correlation with dendritic spine density. *J. Neurosci.* **17**, 1848–1859.

Supplemental Materials

Supplemental Experimental Procedures

Preparation of synaptic, cytoplasmic and nuclear fractions

Adult male rats were deeply anesthetized with ethyl ether and decapitated. The brains were removed and placed in ACSF. Note that the same hippocampal slices were used in order to directly compare with spine morphology and electrophysiology investigations. Whole tissues (not slices) were used for hypothalamus, cerebral cortex and cerebellum. Fractionation was performed by a combination of centrifugations at 4 ˚C for the hippocampus, hypothalamus, cerebral cortex and cerebellum (Cohen et al., 1977). Slices or tissues were homogenized in 0.32M sucrose in 1 mM $NaHCO_3$, 1 mM $MgCl_2$, 0.5 mM $CaCl_2$ with protease inhibitors 0.5 mM PMSF and 0.1mM leupeptin, and centrifuged at 1,400 g for 10 min. The pellet was centrifuged again in the same solution. The pellet was used as the nuclear fraction (P1 fraction). Supernatant from the first centrifugation was subjected to centrifugation at 10,000 g for 20 min. The retrieved pellet (P2 fraction) was further purified with sucrose density gradient centrifugation. The pellet was suspended in 0.32M sucrose in 1mM $NaHCO_3$ and overlaid on 0.85/1.0/1.2 M sucrose step gradient. The sample was ultracentrifuged at 82,500 g for 120 min. The synaptosomal fraction was collected from the interface between 1.0M and 1.2M sucrose. Purification of the 'PSD fraction' was performed as follows. Synaptosomal fraction was treated with 1% Triton X-100 in 12mM Tris-HCl (pH 8.1), and Triton-insoluble pellet fraction were collected by centrifugation at 32,800 g for 20 min. The pellet was suspended in 0.32M sucrose in 1mM $NaHCO_3$ and overlaid on 1.0/1.5/2.1 M sucrose step gradient. The sample was ultracentrifuged at 201,800 g for 120 min. Crude PSD fraction was collected from the interface between 1.5 M and 2.1 M sucrose, and then suspended in 150mM KCl with 1% TritonX-100. The suspension was centrifuged for 20min at 201,800g, and the pellet was collected as purified PSD fraction. To obtain the 'presynaptic membrane-enriched fraction' (low density synaptic membrane fraction), the supernatant obtained from fractionation of P2 was centrifuged at 25000 g for 60 min. Resultant supernatant was centrifuged again at 100,000 g for 60 min, and the pellet and the supernatant was collected separately as the presynaptic membrane-enriched fraction and the cytoplasmic fraction, respectively. For investigations of ERαKO mice, homogenates of the whole hippocampus

and other brain regions were used, without further purification.

Mass spectrometric analysis of RC-19 reacted ERα

To perform immunoprecipitation with RC-19, hippocampal cytoplasmic fraction (1 mg/mL) was suspended 5 mM HEPES buffer, containing 25mM KCl, 4mM EDTA-4Na, 0.5% Triton X-100, 1mM Na_3VO_4, 50mM NaF. Twenty μL of protein G-Sepharose beads (Sigma) covalently coupled with 10μg of RC-19 by dimethyl pimelimidate-2HCl (Pierce) was incubated with 15 mg protein overnight at 4°C. The beads were eluted with sample buffer of SDS-PAGE for 5min at 100 °C, and reduced with 100 mM DTT for 10 min. The eluted immunoprecipitant proteins were suspended in 125 mM Tris-HCl buffer (pH 6.8), containing 5 mM 2-mercaptoethanol, 10% sucrose, 6% SDS and 0.002% bromophenol blue, and subjected to SDS-PAGE using a 10% polyacrylamide gel. After protein separation, the gel was stained overnight with 0.1% silver using Silver stain MS kit (Wako, Japan). A silver stained band with approxi. 67 kDa was excised from the gel, destained with destaining solution of Silver stain kit, and the proteins were digested in-gel with trypsin. Digested peptides were extracted from gel pieces with 50 μl of 50% acetonitrile and 0.1% trifluoroacetic acid. Zip Tip C18 microcolumn (Millipore) was used for purification of peptides. MALDI-TOF mass-spectrometric analysis was performed on an ultraflex time-of-flight instrument (Bruker Daltonics) equipped with a nitrogen laser operating at 337 nm. All MALDI-TOF results were obtained in the positive reflector mode using a-cyano-4-hydroxycinnamic acid (saturated solution in 50 % acetonitrile with 0.1% trifluoroacetic acid) as the matrix. Samples were prepared by mixing 0.5 μL of peptide solution with 0.5 μL of matrix soln. on a MALDI plate and allowed to air dry before inserting into the spectrometer. Mass spectra were calibrated with angiotensin II (1046.54 Da), angiotensin I (1296.68 Da), substance P (1347.74 Da), bombesin (1619.82 Da), adrenocorticotropic hormone (ACTH18-39) (2465.20 Da), and insulin (5733.54 Da). All masses are reported as monoisotopic mass values. In addition, peptides derived from trypsin (843.02 and 2212.44 Da) were used for validation. Peptides were identified by using the Mascot search program (http://www.matrixscience.com) to perform theoretical trypsin digests and searching for potential unmodified tryptic peptides (with up to one missed cleavages) or suspected modified species.

Methionine residues were considered as either normal Met or their oxidized form (Met-ox), and cysteine residues were considered to be carbamidomethylated (C-cam) or reacted with acrylamide to produce Cys-*S*-b-propionamide (C-pam).

RT-PCR and Southern hybridization

Specific primer pairs for subregions of ERα exons were as follows:
Exon 1'-2-3-4' (from 423 to 1011 bp);
Forward; 5'-GGGGCCTCGGCTCCGGTCTATGG-3', a sequence in exon 1,
Reverse; 5'-TCCCTCCTCGGCGGTCTTTTCGTA-3', a sequence in exon 4
Exon 3'-4-5' (from 943 to 1409 bp);
Forward; 5'-GCCGGCTGCGCAAGTGTTACG-3', a sequence in exon 3,
Reverse; 5'-GGAGCGCCAGACCAGACCAATCA-3', a sequence in exon 5
Exon 4'-5-6' (from 1073 to 1496 bp);
Forward, 5'-AGGAGACATGAGAGCTGCCAACC-3', a sequence in exon 4,
Reverse, 5'-GATCTCCACCATGCCTTCTACACA-3', a sequence in exon 6,
Exon 5'-6-7' (from 1321 to 1735 bp);
Forward, 5'-GCTTTGGGGACTTGAATCT-3', a sequence in exon 5,
Reverse, 5'-AGACGGCGATGCTGTTGC-3' sequence in exon 7
Exon 6'-7-8' (from 1540 to 1980 bp);
Forward, 5'-ACCTGCAGGGAGAAGAGTTTGT-3', a sequence in exon 6
Reverse, 5'-GGGGGATGTAGTAGGTTTGTAAGG-3', a sequence in exon 8
Specific primer pairs for ERβ were designed as follows:
Forward; 5'-GCAAACCAGGAGGCAGAAAGTAGC-3',
Reverse; 5'-AAGTGGGCAAGGAGACAGAAAGTAAGTA-3'.
Using these primer pairs, both two subtypes of ERβ1 and ERβ2 mRNAs were detectable. The PCR protocols comprised application of a 30 sec denaturation period at 95°C, a 20 sec annealing period at 68°C (ERα), 65°C (ERβ) and a 30 sec extension at 72°C, for 34 cycles (ERα) or 36 cycles (ERβ).

Supplemental Discussion

Previous understanding of ERα from mRNA and ligand binding studies

The expression level of ERα mRNA in adult hippocampus obtained from the current and previous RT-PCR investigations is significant at levels as high as approx. 0.5 fold of that in the neonatal stage (Ivanova and Beyer 2000; Solum and Handa 2001). *In situ* hybridization studies, in general (Shughrue et al. 1997; Laflamme et al. 1998) have detected low levels of ERα mRNA throughout the adult hippocampus with signals found mostly over the cell body layers of CA1, CA3 and the dentate gyrus. An exception is an *in situ* hybridization study which has indicated a distribution mainly in the interneurons of both the neonatal and adult hippocampus (Orikasa et al. 2000). A recent *in vivo* ligand-binding study using autoradiography of [^{125}I]estrogen with a high radioactivity showed labeling of more cells than previously been detected using low radioactive [^{3}H]estradiol (Shughrue and Merchenthaler 2000). The [^{125}I]estrogen labeling has shown rather a few interneuron-like cells in dorsal CA1, some principal cells in dorsal CA3, and a large number of principal cells in middle and ventral hippocampus (Shughrue and Merchenthaler 2000). The number of [^{125}I]estrogen labeled cells are, however, significantly less than RC-19 labeled cells. Although we do not have a good explanation to this at the moment, high concentration of hippocampus-derived estradiol (Hojo et al. 2004) might interfere the binding of [^{125}I]estrogen derived from the blood circulation. In the experiments [^{125}I]estrogen was injected subcutaneously at 1-2μg/kg (2.5-5 nM), therefore, the actual concentration of [^{125}I]estrogen reached the hippocampus might be much lower, due to a significant loss at the blood brain barrier. Therefore, we may need to perform ligand-binding study by direct application of [^{125}I]estrogen to isolated hippocampal slices. In addition, even with [^{125}I]estrogen, clear synaptic labeling of ERα may be extremely difficult, because [^{125}I]estrogen would diversely distribute on the synaptic membranes and the amount of ERα at synapses would be very small compared with nuclear and cytoplasmic ERα as judged from Western blot analysis using RC-19 (see Fig. 3).

The observed level of ERα mRNA in adult rat hippocampus was as high as approx. 56% of P10 rat, the reactivity of AS409 in many

immunohitochemical studies of adult hippocampus seems much lower than those expected from the mRNA level. In this sense, a significant RC-19-immunoreactivity in Fig. 4 would be in good coincidence with ERα mRNA level.

Chronic and genomic effect of estradiol via nuclear ERα

Although extensive investigations have been performed on the chronic, delayed effects of estradiol on the synaptic plasticity of female rat hippocampus, the distribution of nuclear estrogen receptors by which these modulations may be effected, has remained uncertain particularly in glutamatergic neurons. The chronic action of estradiol has previously been investigated mainly in female rats, in relation to the modulation of circulatory estrogen levels (Woolley and McEwen, 1994; Bi et al., 2001). The dendritic spine density in CA1 pyramidal neurons is sensitive to experimentally-induced estrogen depletion and replacement (Woolley et al., 1997; Bi et al., 2000). Evidence suggests that estradiol mediates these spine density changes through NMDA receptors (Woolley and McEwen, 1994; Woolley et al., 1997), and that these morphological changes are blocked by NMDA receptor antagonists (Woolley and McEwen, 1994).

The electrophysiological properties of synaptic transmission are enhanced by several days of treatment of cultured hippocampal slices with estradiol (Pozzo-Miller et al., 1999). Explanation of these morphological changes in pyramidal neurons has been performed by disinhibition of pyramidal neurons via GABAergic interneurons, because nuclear ERα receptors had previously been observed mainly in interneurons with AS409 and MC-20 staining. The current observation of nuclear ERα in principal neurons of CA1, CA3 and DG represents supporting evidence for the hypothesis that estradiol mediates the delayed morphological changes, via ERα in glutamatergic neurons.